HHS Public Access

Author manuscript

Eur Radiol. Author manuscript; available in PMC 2017 December 28.

Published in final edited form as:

Eur Radiol. 2016 June ; 26(6): 1792–1800. doi:10.1007/s00330-015-3972-0.

Chemical Exchange Saturation Transfer (CEST) MR technique for in-vivo liver imaging at 3.0 Tesla

Shu-Zhong Chen[1], **Jing Yuan**[2], **Min Deng**[1], **Juan Wei**[3], **Jinyuan Zhou**[4,5], and **Yì-Xiáng J Wáng**[1]

[1]Department of Imaging and Interventional Radiology, Faculty of Medicine, The Chinese University of Hong Kong, Prince of Wales Hospital, Shatin, New Territories, Hong Kong SAR

[2]Medical Physics and Research Department, Hong Kong Sanatorium & Hospital, Happy Valley, Hong Kong SAR

[3]Philips Healthcare Asia, Shanghai, China

[4]Department of Radiology, Johns Hopkins University, Baltimore, MD, USA

[5]F.M. Kirby Research Center for Functional Brain Imaging, Kennedy Krieger Institute, Baltimore, MD, USA

Abstract

Purpose—To evaluate Chemical Exchange Saturation Transfer (CEST) MRI for liver imaging at 3.0-T.

Materials and Methods—Images were acquired at offsets (n=41, increment=0.25ppm) from −5 to 5ppm using a TSE sequence with a continuous rectangular saturation pulse. Amide proton transfer-weighted (APTw) and GlycoCEST signals were quantified as the asymmetric magnetization transfer ratio (MTR_{asym}) at 3.5ppm and the total MTR_{asym} integrated from 0.5 to 1.5ppm, respectively, from the corrected Z-spectrum. Reproducibility was assessed for rats and humans. Eight rats were devoid of chow for 24-hours and scanned before and after fasting. Eleven rats were scanned before and after one-time CCl4 intoxication.

Results—For reproducibility, rat liver APTw and GlycoCEST measurements had 95% limits of agreement of −1.49% to 1.28% and −0.317% to 0.345%. Human liver APTw and GlycoCEST measurements had 95% limits of agreement of −0.842% to 0.899% and − 0.344% to 0.164%. After 24-hours fasting rat liver APTw and GlycoCEST signals decreased from 2.38±0.86% to 0.67±1.12% and from 0.34±0.26% to −0.18±0.37% respectively ($p<0.05$). After CCl4 intoxication rat liver APTw and GlycoCEST signals decreased from 2.46±0.48% to 1.10±0.77%, and from 0.34±0.23% to −0.16±0.51% respectively ($p<0.05$).

Conclusion—CEST liver imaging at 3.0-T showed high sensitivity for fasting as well as CCl4 intoxication.

Corresponding to: Dr Yì-Xiáng J Wáng, Department of Imaging & Interventional Radiology, The Chinese University of Hong Kong, Shatin, New Territories, Hong Kong SAR. yixiang_wang@cuhk.edu.hk, tel (852) 2632 2289, fax (852) 2636 0012.

The scientific guarantor of this publication is Dr Yi-Xiang Wang. Dr Juan Wei is an employee of Philips Healthcare. The other authors declare no conflict of interest.

Keywords

Magnetic resonance imaging; Chemical Exchange Saturation Transfer (CEST); Liver; Glycogen; Amide Proton Transfer (APT)

Introduction

Chronic liver diseases, including simple steatosis (SS), nonalcoholic steatohepatitis (NASH), and liver fibrosis are major public health problem worldwide [1]. Nonalcoholic steatohepatitis (NASH) can lead to liver cirrhosis, terminal liver failure, and hepatocellular carcinoma. Clinically, patients with diffuse liver diseases can remain asymptomatic or have only mild, nonspecific symptoms until the development of cirrhosis. To date, noninvasive diagnostic tests available from clinical practice are not sensitive or specific enough to detect occult liver injury at early or intermediate stages. The reliability of liver function tests, serological tests of specific serum makers, and liver stiffness measurement in assessing liver fibrosis is still under investigation [2-6]. Liver biopsy is currently the standard of reference for the diagnosis and staging of liver fibrosis. However, it is an invasive procedure with possible complications [7]. Histological assessment of fibrosis is also an inherently subjective process, and it is subject to sampling variability. The extent of variations from observer interpretation by expert histopathologists may be as high as 20% [8]. These limitations make liver biopsy somewhat suboptimal for diagnosis and longitudinal monitoring in the general population. A noninvasive and quantitative technique for assessing liver fibrosis and monitoring disease progression or therapeutic intervention is highly desirable.

Chemical exchange saturation transfer (CEST) has been proposed as a novel MRI contrast mechanism in recent years and been actively explored for a variety of clinical applications [9-13]. CEST MRI shares similar theoretical principle as T_1rho MRI, while shows the great advantages of high specificity to certain biochemistry components such as protein [9,10], glycosaminoglycan (GAG), glycogen [14], glutamate [15] and glucose [16,17]. In 2003 Zhou *et al* first demonstrated pH-sensitive amide proton transfer (APT) effects during several physiological alterations in the rat brain, as well as the possibility of producing protein-based APT-weighted (APTw) contrast in the rat 9L gliosarcoma model at 4.7T [9]. After showing the existence of APT effects in animal models, Jones *et al* applied the APT technique to patients with brain tumours in 2006 [18]. This and many subsequent studies by Zhou *et al* have clearly shown that APT imaging for malignant brain tumours has much potential [19, 20]. In 2007, van Zijl *et al* proposed the principle of endogenous GlycoCEST imaging and demonstrated that glycogen in the excised perfused mouse liver was detectable at 4.7T [14]. In 2008, Ren *et al* [21] demonstrated the distribution of glucose in livers using an exogenous paramagnetic CEST sensor, also on perfused mouse liver at 4.7T. Recently, Sagiyama *et al* [22] for the first time reported the feasibility of *in vivo* GlycoCEST imaging in mice at 9.4T, and the observed temporal change in the MTR_{asym} at 1.25 ppm was suggested to reflect the alteration of hepatic glycogen levels by fasting and/or re-feeding. Bawden *et al* [23] reported that PRESS-CEST spectroscopy offers a promising new technique of simultaneously measuring local glycogen and lipid levels *in vivo* at 3T.

To facilitate the use of CEST MRI for routine clinical use, a number of critical issues remain to be addressed. The feasibility of GlycoCEST imaging for *in-vivo* liver has not been demonstrated at relatively lower magnetic field strength for clinical scanners, such as 1.5T and 3T, where the GlycoCEST MR signal supposes to be much lower than at dedicated ultra-high field MRI scanner for research. Meanwhile, GlycoCEST signal at clinical field strength is more likely to be contaminated by direct saturation (DS) of water and other CEST pools resonating at proximate frequencies due to the smaller absolute chemical shift. The reproducibility of GlycoCEST imaging for liver is crucial for its potential use as a reliable clinical imaging biomarker, but has not yet been examined so far. In this study we also attempted to evaluate whether CEST imaging, including GlycoCEST and APTw MRI, is sensitive to detect the pathological variation of liver induced by intoxication on rats. For these purposes, the aim of the current 3.0-T MRI study is to evaluate the feasibility and reproducibility of CEST imaging for both human and animal in-vivo liver imaging, and to evaluate the sensitivity of CEST imaging to fasting and carbon tetrachloride (CCl4) intoxication on rats.

Materials and Methods

Animal study

Nineteen male Sprague-Dawley rats with a weight of 200–250g were used in the study. The protocols and procedures were approved by the local Animal Experimentation Ethics Committee. Two to three animals were housed per stainless steel cage on a 12-h light/12-h dark cycle in an air-conditioned room at 22°C, and checked daily by the animal care staff. A standard commercial rat chow (Prolab RMH 2500, PMI Nutrition International LLC, Brentwood, USA) and water were available *ad libitum*.

For the scan-rescan reproducibility study, each rat was examined twice with an interval of two weeks. For the fasting study, eight rats were randomly selected and not fed (rat chow) for 24 hours, but had free access to water. These rats were scanned twice before fasting and after fasting. The remaining 11 rats underwent liver carbon tetrachloride (CCl4) intoxication study. Liver intoxication induced by intraperitoneal injection of 1 ml kg^{-1} body weight CCl4, with a 1:1 volume mixture of CCl4 (99.8%; BDH Laboratory, Poole, UK) in olive oil [24]. These rats were scanned before and 48 hours after CCl4 administration.

All rats were scanned using a Philips Achieva 3T scanner (Philips Healthcare, Best, the Netherlands) with a body coil for transmission and a wrist coil for reception. Anesthetized was used by using a combination of xylazine (Rompun; Bayer HealthCare, Leverkusen, Germany) 10 mg per kilogram of body weight and ketamine (Ketalar; Pfizer, Hong Kong SAR) 90mg/kg. Conventional T_2-weighted images were acquired by 2D multiple slice turbo-spin-echo (TSE) sequence to localize the anatomy, with TSE factor =16, TR/TE=2083 ms/80 ms; field of view (FOV)=80×65 mm^2; slice thickness=2mm; and pixel size=0.5×0.5 mm^2. Then CEST images acquisition was performed using a single-slice TSE sequence with chemical shift-selective fat suppression [25, 26]. A continuous rectangular RF pulse was performed for saturation, with a B_1 field strength of 3 μT and a fixed duration of 300 ms. Major imaging parameters were as follows: TSE factor=11, TR=2350 ms; TE=6 ms; FOV=80×65 mm^2; pixel size=1.25×1.25 mm^2; slice thickness=2mm; number of signal

averages (NSA)=5. Baseline image was obtained first without using saturation pulse, and then the saturated images were acquired at the offsets of 0, ±0.25, ±0.5, ±0.75, ±1, ±1.25, ±1.5, ±1.75, ±2, ±2.25, ±2.5, ±2.75, ±3, ±3.25, ±3.5, ±3.75, ±4, ±4.25, ±4.5, ±4.75, ±5 parts per million (ppm). The total data acquisition time was 16 min and 31 sec. Consecutive CEST images demonstrated rat liver position remained consistent during the data acquisition at different offsets (Supplement Fig 1)

Human volunteer study

Eight volunteers comprising 6 males and 2 females with a mean age of 30 yrs (range: 23–47 yrs) participated in this study. All subjects were clinically healthy, with no liver disease history or alcoholism. The study was approved by the local human research ethics committee, and all subjects provided written informed consent. MRI data were acquired with the same 3T scanner. An 8-channel cardiac coil was used as the signal receiver, and a body coil was used as radiofrequency transmitter. After using conventional T_2-weighted images (TSE factor=54; TR/TE=1236 ms/70 ms; FOV=160×280 mm^2; slice thickness=4 mm; pixel size=1 × 1.5 mm^2) to localize the anatomy, the human liver CEST image were acquired using a single-slice TSE sequence with chemical shift-selective fat suppression. Major CEST imaging parameters were as follows: TSE factor=16; TR=2350 ms; TE=6 ms; FOV=160×280 mm^2; pixel size=2 × 2 mm^2; slice thickness=4 mm; NSA=1; the total data acquisition time was 4 min and 58 sec; other parameters were identical to those used for animal study. The images were acquired with a breath-hold technique. Volunteers were required to maintain breath-holding at a similar breathing depth during image acquisition. Each volunteer was scanned twice in the morning after a light breakfast, with a time interval of 7 days, to test the reproducibility of CEST MRI.

Z-spectrum analysis

Data analysis was performed using home-developed Matlab (MathWorks, Natick, MA, USA) programs. For the rat study, excluding observable artefacts and blood vessels, five regions-of-interest (ROIs) of approximately 3–4 mm^2 were first manually placed on the liver parenchyma region of the T2 weighted image and then the ROI mask was transferred to the CEST image (Fig. 1A,B). All the rat data were measured by independently by two radiologists with animal research experience. For the human study, five ROIs of approximately 200–300 mm^2 were manually placed on the liver parenchyma region of CEST image with the same method of the rat study (Fig. 1B) [25]. For each voxel, the Z-spectrum was first least-square fitted by a 12th-order polynomial model and interpolated to a finer resolution of 0.001 ppm. The actual water resonance was assumed to be at the frequency associated with the lowest intensity of the fitted Z-spectrum. Then, the interpolated Z-spectrum was shifted to the 0 ppm of the offset axis to correct for the field heterogeneity ΔB_0 [11]. The magnitude of the CEST effect was quantified as a magnetization transfer asymmetry ratio (MTR_{asym}):

$$MTR_{asym}(\Delta\Omega) = \frac{S(-\Delta\Omega)}{S_0} - \frac{S(\Delta\Omega)}{S_0}$$

where ΔΩ denotes the shift difference between irradiation frequency and the water resonance, and S and S_0 are the saturated and nonsaturated image intensities, respectively. The MTR_{asym} at 3.5ppm was quantified as APT-weighting (APTw) value [10] and the mean MTR_{asym} in the frequency range ΔΩ=0.5 to 1.5 ppm was quantified as GlycoCEST value [22, 23]. The voxel-wise coefficient of determination R^2 was also calculated to evaluate the goodness-of-fit of Z-spectrum fitting. The voxel which showed relatively poor goodness-of-fit (R^2<0.99) would be excluded from analysis.

All MRI were measured independently by two radiologists with research experience. For the rat study, the inter-reader agreement ICC (Intraclass correlation coefficient) was 0.893 for APTw measurement and 0.870 for GlycoCEST measurement. For the human study, ICC was 0.844 for APTw measurement and 0.867 for GlycoCEST measurement. All indicated good inter-reader agreement. For consistency, one reader's results were presented in the results.

Data were expressed as a mean ± standard deviation (SD). All statistical analyses were performed using SPSS 14.0 (SPSS Inc., Chicago, IL, USA), Wilcoxon signed rank test was used for comparison. All statistical tests were two-sided. A *P* value of <0.05 was considered statistically significant.

Results

1. Rat liver APTw and GlycoCEST MR scan-rescan reproducibility

Three rats (3/19) were excluded from analysis because of motion artefacts due to anaesthesia failure. For the remaining sixteen rats, the values of the APTw difference and GlycoCEST difference between the two scans were plotted against the mean MTR_{asym} of these two scans with the Bland-Altman plot. For APTw measurement, scan-rescan 95% limits of agreement ranged from −1.49% to 1.28% with a mean difference of −0.110% (Fig. 2A). For GlycoCEST measurement, scan-rescan 95% limits of agreement ranged from −0.317% to 0.345% with a mean difference of 0.014% (Fig. 2B). One B_0 shift map of a rat with 5 ROIs selected is shown by Supplement Fig 2.

2. APTw and GlycoCEST measurements before and after 24-hour fasting

The results of pre-fasting and post-fasting APTw measurement and GlycoCEST measurement in eight rats are shown in Fig 3. The post-fasting APTw value decreased from 2.38±0.86% to 0.67±1.12% (p=0.012). The mean GlycoCEST measurement also decreased after fasting (0.34±0.26% to −0.18±0.37%, p=0.012).

3. APTw and GlycoCEST measurements 48-hour after CCl4 injection

The results of CCl4 injection on liver APTw and GlycoCEST measurements are shown in Fig. 4. The baseline APTw value was 2.46±0.48% and the GlycoCEST value was 0.34±0.23%. 48 hours after CCl4 intoxication, the liver APTw value was reduced to 1.10±0.77% (p=0.004), and the GlycoCEST value was reduced to −0.16±0.51% (p=0.02). After 48 hours of CCl4 intoxication, the MTR_{asym} value presented observable decrease in both APTw image, GlycoCEST image and the corresponding MTR_{asym} spectrum.

4. Human liver APTw and GlycoCEST MR scan-rescan reproducibility

CEST data were successfully acquired in all 8 subjects (Fig. 5). The values of the APTw difference and GlycoCEST difference between the two scans in human liver were plotted against the mean MTR_{asym} of these two scans in the Bland-Altman plot (Fig. 6). For APTw, scan-rescan 95% limits of agreement ranges from −0.842% to 0.899% (mean difference: 0.029%). For GlycoCEST, scan-rescan 95% limits of agreement ranges from - 0.344% to 0.164% (mean difference: −0.089%). This study showed the liver parenchyma APTw and GlycoCEST values were 1.66±0.48% and 0.46±0.45% respectively in the morning after light breakfast. One B_0 shift map of a human subject with 5 ROIs selected is shown by Supplement Fig 3.

Discussion

In patients with diffused liver diseases, the liver parenchyma usually has a normal appearance or may exhibit only subtle, nonspecific heterogeneity on conventional MR images. A number of MR imaging techniques have been investigated to assess early liver parenchyma fibrosis, including T_1rho imaging [27-31], tagged MRI assessing liver strain [32], MR elastography [33, 34] and intravoxel incoherent motion (IVIM) technique [35, 36]. Our current study for the first time demonstrated the feasibility and evaluated the reproducibility of CEST imaging of *in-vivo* liver at the clinical field strength of 3T in both rats and human. Agreed well with the previous *in-vivo* liver GlycoCEST studies [22, 23], positive GlycoCEST MTR_{asym} was observed in both rat and human before fasting, and GlycoCEST MTR_{asym} reduced considerably after 24-h fasting in rat. This reduction of GlycoCEST MTR_{asym} after fasting is believed to reflect the reduction of hepatic glycogen levels. In addition, we also observed the significant drop GlycoCEST MTR_{asym} in the CCl4 intoxicated rat livers. The histopathological course of CCl4 intoxication has been well illustrated [24, 37, 38]. 48-hr after CCl4 intoxication, the liver is associated with a great extent of inflammation, oedema and tissue necrosis, and involving metabolic activation, reactive free radical metabolites, lipid peroxidation, covalent binding and disturbance of calcium homeostasis. According to Muriel [39], in the CCl4 intoxicated rat liver, glycogen content decreased significantly compared to the normal liver, while lipid peroxidation and collagen content increased. This well supported the finding of the reduced GlycoCEST value after CCl4 insult in our study.

Besides the GlycoCEST effect, positive MTR_{asym} at 3.5ppm was also found in both rat and human livers. Although this MTR_{asym} was termed as APTw by convention due to its Z-spectrum location at 3.5ppm in the study, the chemical component source and mechanism attributed to this MTR_{asym} should be carefully assessed further. Ceramides (Cers) might be postulated to contribute to this MTR_{asym}, which are a lipid species that exert biological effects in nonalcoholic fatty liver disease through cellular proliferation, differentiation, and cell death [40]. However, since fat suppression was applied prior to acquisition, this MTR_{asym} should not be dominated by the contamination of lipid at − 3.5ppm, the opposite side on Z-spectrum [41]. Furthermore, according to Figs. 3 and 4, two z-spectra overlapped relatively well on the right. Therefore, the contribution of possible upfield nuclear Overhauser enhancement (NOE) effects to the MTR_{asym} difference should be small [42, 43].

According to a 500MHz proton NMR study of Cer and its analogues in deuterated chloroform (CDCl3) at 25°C by Li *et al* [44], -NH in Cers has a chemical shift of ~6.3ppm, about 1.6ppm relative to water (4.7ppm chemical shift). Considering the lower resonance of 128MHz at 3T and the observation of broad baseline positive MTR_{asym} peak above 1.5ppm (blue curves in Figs 3b and 4b), it is possible that – NH has concomitant spill-over effects at higher chemical shifts and induces positive MTR_{asym}. On the other hand, it was found by Ichi *et al* [45] that ceramide in the liver and plasma increased after CCl4 intoxication in the rat. It seems conflicting with the reduction of APTw MTR_{asym} observed in our study. It may be explained by that Cers are more dissolvable in Chlorine solvent so that CCl4 might deplete the exchangeable protons of Cers with water. Nevertheless, these postulations have to be further carefully examined and verified in future studies.

It is known that the measured CEST signal intensity in tissue is related to the mobile proton content, the proton exchange rate (depending on tissue pH), and several tissue and experimental factors. As such, the measured MTR_{asym} for both GlycoCEST and APTw may only reflect the comprehensive overall change in liver but cannot delineate the individual contribution from each factor. Meanwhile, the quantified MTR_{asym} signal intensity is more or less contaminated by the upfield NOE effect [46]. In addition to changes in labile pool concentration, the decrease in MTR_{asym} observed after intoxication might be attributed to residual T_1 and T_2 effects through the spillover and conventional MT. However, based on some recent studies [20, 47], the upfield NOE effect is generally the minor contributor to the MTR_{asym}-based CEST image signal with a B_1 field strength of 3 μT. According to Chow et al [48], T_1 and T_2 relaxation times of mice were observed significantly increase after two weeks of CCL4 intoxication at 7T. However, the short-term variation of T1 and T2 after 48 hours of CCL4 intoxication has not been investigated and is still unknown. Quantitative T_1 and T_2 mapping, which were not conducted in this study, may be helpful to further delineate the contributing factors for CEST imaging in future studies. In this study, 12^{th}-order polynomial fitting and interpolation were applied for MTR_{asym} quantification because the acquired Z-spectra were generally smooth due to the relatively small endogenous CEST contrast at clinical field strength of 3T. Excellent goodness-of-fit was achieved. Meanwhile, the acquired Z-spectra under the saturation field strength of 3μT were relatively flat rather than sharp in shape so the even higher order polynomial fitting might not be necessary. Cubic-spline interpolation [49] has been reported to improve MTR_{asym} quantification particularly for CEST images at low SNR, so should be useful in future studies when lower saturation strength is used with low NSA. Water saturation shift referencing (WASSR) has been proposed for better glycoCEST MTR_{asym} quantification by offering more precise ΔB0 map and remarkable improvement has been demonstrated for the stationary tissue of human calf muscle at 3T [50]. However, the WASSR acquisition and quantification might be highly sensitive to motion because of the extremely low saturation strength and thus the sharp Z-spectrum. Furthermore, in the presence of uneven respiration cycle, the use of WASSR-derived ΔB0 map for Z-spectrum correction might also be technically challenging. It is recognized that our approach in this study without WASSR would definitely compromise the accuracy of the estimated MTR_{asym}. Consequently, the utilization of WASSR in moving organs like liver should be further explored. Besides MTR_{asym} for Z-spectrum analysis,

alternative data processing approaches for better quantifying CEST signal [47, 51-54] may also be used to investigate pathological alteration of liverin the future.

It is also worth noting that the measured MTR_{asym} depends also on the saturation pulse strength and duration. Ideally, the saturation pulse should be optimized based on both hardware capability and proton exchange rate in tissue. The Glycogen proton exchange rate is estimated faster than amide proton exchange rate, so a slightly higher saturation strength of 3μT was used in this study than the optimized 2μT for APTw imaging as observed in previous brain studies [20]. Meanwhile, the longest saturation duration of 300ms that was achievable on our clinical MRI scanner was applied to approach complete direct saturation. Nevertheless, as GlycoCEST effect is closer to the water resonant frequency, the MTR_{asym} of GlycoCEST values might be more likely contaminated by direct saturation and magnetization transfer effect under high power saturation. Therefore, future study on saturation pulse optimization is warranted by investigating how the magnitudes of APTw and GlycoCEST signal change with different saturation powers.

This current study is a first time proof-of-principle *in-vivo* study for liver CEST imaging at clinical field strength, and there are a few limitations. The time course of the liver CCl4 intoxication has not been performed. The human subject study was limited to a small number of volunteers. Strategies to shorten acquisition time while maximize CEST contrast-to-noise ratio should be investigated [49, 55-60]. The origin of CEST effect at nominal APT resonance should be further explored. Further evaluations are needed to correlate CEST MRI signal and hepatic concentration of glycogen in conditions of varying temperature, pH or structure of glycogen. Since T_{1rho} and CEST technique share similar theoretical principle and T_{1rho} has been demonstrated to be sensitive to detect early stage liver fibrosis [29, 30], further comparative study of T_{1rho} vs. CEST technique will be of interest.

In summary, this study for the first time showed both APTw and GlycoCEST MR liver imaging on a clinical 3.0 T system is feasible for both rats and human subjects. Both APTw and GlycoCEST MR measurements showed high sensitivity for fasting as well as CCl4 intoxication. To translate CEST MR imaging into a practical tool and thereby positively influence clinical management, technological advancement including acceleration of data acquisition and improvement in contrast-to-noise ratio remain to be further exploited. The mechanism of APTw and GlycoCEST decrease following fasting as well as CCl4 intoxication remains to be fully explored.

Supplementary Material

Refer to Web version on PubMed Central for supplementary material.

Acknowledgments

The authors also thank two reviewers for their insightful comments, and Dr *BLINDED* for image processing during the revision process.

This study was partially by grants from the Research Grants Council of the Hong Kong SAR (Project No 476313 Project No. SEG_CUHK02) and the National Institutes of Health (R01EB009731, R01CA166171). No complex statistical methods were necessary for this paper. Institutional Review Board approval was obtained. Written informed consent was obtained from all subjects in this study. Approval from the institutional animal care

committee was obtained. No study subjects or cohorts have been previously reported. Methodology: experimental, performed at one institution.

References

1. Wallace K, Burt AD, Wright MC. Liver fibrosis. Biochem J. 2008; 411:1–18. [PubMed: 18333835]
2. Patel K, Shackel NA. Current status of fibrosis markers. Curr Opin Gastroenterol. 2008; 30:253–9.
3. Anania C, Pacifico L, Ferraro F, Olivero E, Chiesa C. Aspartate transaminase to platelet ratio index (APRI) to assess liver fibrosis in patients with chronic liver disease. Hepat Mon. 2011; 11:479–80. [PubMed: 22087183]
4. Tatsumi C, Kudo M, Ueshima K, Kitai S, Takahashi S, Inoue T, Minami Y, Chung H, Maekawa K, Fujimoto K, Akiko T, Takeshi M. Noninvasive evaluation of hepatic fibrosis using serum fibrotic markers, transient elastography (FibroScan) and real-time tissue elastography. Intervirology. 2008; 51(Suppl 1):27–33. [PubMed: 18544945]
5. Sy S, Huang S, Wang YX, Yu J, Ahuja AT, Zhang YT, Pickwell-MacPherson E. Terahertz spectroscopy of liver cirrhosis: investigating the origin of contrast. Phys Med Biol. 2010; 55:7587–96. [PubMed: 21098916]
6. Ligabue G, Besutti G, Scaglioni R, Stentarelli C, Guaraldi G. MR quantitative biomarkers of non-alcoholic fatty liver disease: technical evolutions and future trends. Quant Imaging Med Surg. 2013; 3:192–5. [PubMed: 24040614]
7. Janes CH, Lindor KD. Outcome of patients hospitalized for complications after outpatient liver biopsy. Ann Intern Med. 1993; 118:96–98. [PubMed: 8416324]
8. Bravo AA, Sheth SG, Chopra S. Liver biopsy. N Engl J Med. 2001; 344:495–500. [PubMed: 11172192]
9. Zhou J, Lal B, Wilson DA, Laterra J, van Zijl PCM. Amide proton transfer (APT) contrast for imaging of brain tumors. Magn Reson Med. 2003; 50:1120–1126. [PubMed: 14648559]
10. Zhou J, Payen J, Wilson DA, Traystman RJ, van Zijl PCM. Using the amide proton signals of intracellular proteins and peptides to detect pH effects in MRI. Nat Med. 2003; 9:1085–1090. [PubMed: 12872167]
11. Yuan J, Chen S, King AD, Zhou J, Bhatia KS, Zhang Q, Yeung DK, Wei J, Mok GS, Wang YX. Amide proton transfer-weighted imaging of the head and neck at 3 T: a feasibility study on healthy human subjects and patients with head and neck cancer. NMR Biomed. 2014; 27:1239–47. [PubMed: 25137521]
12. Kim M, Chan Q, Anthony MP, Cheung KM, Samartzis D, Khong PL. Assessment of glycosaminoglycan distribution in human lumbar intervertebral discs using chemical exchange saturation transfer at 3 T: feasibility and initial experience. NMR Biomed. 2011; 24:1137–44. [PubMed: 21387446]
13. Haneder S, Apprich SR, Schmitt B, Michaely HJ, Schoenberg SO, Friedrich KM, Trattnig S. Assessment of glycosaminoglycan content in intervertebral discs using chemical exchange saturation transfer at 3.0 Tesla: preliminary results in patients with low-back pain. Eur Radiol. 2013; 23:861–8. [PubMed: 23052643]
14. van Zijl PC, Jones CK, Ren J, Malloy CR, Sherry AD. MRI detection of glycogen in vivo by using chemical exchange saturation transfer imaging (glycoCEST). Proc Natl Acad Sci U S A. 2007; 104:4359–64. [PubMed: 17360529]
15. Cai K, Haris M, Singh A, Kogan F, Greenberg JH, Hariharan H, Detre JA, Reddy R. Magnetic resonance imaging of glutamate. Nat Med. 2012; 18:302–306. [PubMed: 22270722]
16. Chan KW, McMahon MT, Kato Y, Liu G, Bulte JW, Bhujwalla ZM, Artemov D, van Zijl PC. Natural D-glucose as a biodegradable MRI contrast agent for detecting cancer. Magn Reson Med. 2012; 68:1764–73. [PubMed: 23074027]
17. Walker-Samuel S, Ramasawmy R, Torrealdea F, Rega M, Rajkumar V, Johnson SP, Richardson S, Goncalves M, Parkes HG, Arstad E, Thomas DL, Pedley RB, Lythgoe MF, Golay X. In vivo imaging of glucose uptake and metabolism in tumors. Nat Med. 2013; 19:1067–72. [PubMed: 23832090]

18. Jones CK, Schlosser MJ, van Zijl PC, Pomper MG, Golay X, Zhou J. Amide proton transfer imaging of human brain tumors at 3T. Magn Reson Med. 2006; 56:585–92. [PubMed: 16892186]
19. Zhou J, Zhu H, Lim M, Blair L, Quinones-Hinojosa A, Messina SA, Eberhart CG, Pomper MG, Laterra J, Barker PB, van Zijl PC, Blakeley JO. Three-dimensional amide proton transfer MR imaging of gliomas: Initial experience and comparison with gadolinium enhancement. J Magn Reson Imaging. 2013; 38:1119–28. [PubMed: 23440878]
20. Zhou J, Hong X, Zhao X, Gao JH, Yuan J. APT-weighted and NOE-weighted image contrasts in glioma with different RF saturation powers based on magnetization transfer ratio asymmetry analyses. Magn Reson Med. 2013; 70:320–7. [PubMed: 23661598]
21. Ren J, Trokowski R, Zhang S, Malloy CR, Sherry AD. Imaging the Tissue Distribution of Glucose in Livers Using A PARACEST Sensor. Magn Reson Med. 2008; 60:1047–1055. [PubMed: 18958853]
22. Sagiyama K, Zhang S, Dimitrov I, Sherry AD, Takahashi M. In Vivo Monitoring of Liver Glycogen by Chemical Exchange Saturation Transfer Imaging (GlycoCEST) in Live Mice. Proc Intl Soc Mag Reson Med. 2014; 22:0762.
23. Bawden SJ, Mougin O, Hunter K, Marciani L, Gowland P. Simultaneously Measuring Glycogen and Lipid Levels Using Localized CEST Spectroscopy at 3T. Proc Intl Soc Mag Reson Med. 2014; 22:3159.
24. Abe W, Ikejima K, Lang T, Okumura K, Enomoto N, Kitamura T, Takei Y, Sato N. Low molecular weight heparin prevents hepatic fibrogenesis caused by carbon tetrachloride in the rat. J Hepatol. 2007; 46:286–94. [PubMed: 17166617]
25. Sun PZ, Zhou J, Sun W, Huang J, van Zijl PC. Suppression of lipid artifacts in amide proton transfer (APT) imaging. Magn Reson Med. 2005; 54:222–225. [PubMed: 15968669]
26. Lu J, Zhou J, Cai C, Cai S, Chen Z. Observation of true and pseudo NOE signals using CEST-MRI and CEST-MRS sequences with and without lipid suppression. Magn Reson Med. 2014; doi: 10.1002/mrm.25277
27. Deng M, Zhao F, Yuan J, Ahuja AT, Wang YX. Liver T1ρ MRI measurement in healthy human subjects at 3 T: a preliminary study with a two-dimensional fast-field echo sequence. Br J Radiol. 2012; 85:e590–5. [PubMed: 22422392]
28. Zhao F, Yuan J, Deng M, Lu PX, Ahuja AT, Wang YX. Further exploration of MRI techniques for liver T1rho quantification. Quant Imaging Med Surg. 2013; 3:308–15. [PubMed: 24404445]
29. Wang YX, Yuan J, Chu ES, Go MY, Huang H, Ahuja AT, Sung JJ, Yu J. T1rho MR imaging is sensitive to evaluate liver fibrosis: an experimental study in a rat biliary duct ligation model. Radiology. 2011; 259:712–719. [PubMed: 21436087]
30. Wang YX, Yuan J. Evaluation of liver fibrosis with T1ρ MR imaging. Quant Imaging Med Surg. 2014; 4:152–5. [PubMed: 24914415]
31. Allkemper T, Sagmeister F, Cicinnati V, Beckebaum S, Kooijman H, Kanthak C, Stehling C, Heindel W. Evaluation of Fibrotic Liver Disease with Whole-Liver T1ρ MR Imaging: A Feasibility Study at 1.5 T. Radiology. 2014; 271:408–15. [PubMed: 24475807]
32. Mannelli L, Wilson GJ, Dubinsky TJ, Potter CA, Bhargava P, Cuevas C, Linnau KF, Kolokythas O, Gunn ML, Maki J. Assessment of the liver strain among cirrhotic and normal livers using tagged MRI. J Magn Reson Imaging. 2012; 36:1490–5. [PubMed: 22777877]
33. Salameh N, Larrat B, Abarca-Quinones J, Pallu S, Dorvillius I, Leclercq I, Fink M, Sinkus R, Van Beers BE. Early detection of steatohepatitis in fatty rat liver by using MR elastography. Radiology. 2009; 253:90–97. [PubMed: 19587308]
34. Bonekamp S, Kamel I, Solga S, Clark J. Can imaging modalities diagnose and stage hepatic fibrosis and cirrhosis accurately? J Hepatol. 2009; 50:17–35. [PubMed: 19022517]
35. Lu PX, Huang H, Yuan J, Zhao F, Chen ZY, Zhang Q, Ahuja AT, Zhou BP, Wáng YX. Decreases in Molecular Diffusion, Perfusion Fraction and Perfusion-Related Diffusion in Fibrotic Livers: A Prospective Clinical Intravoxel Incoherent Motion MR Imaging Study. PLoS One. 2014; 9:e113846. [PubMed: 25436458]
36. Yoon JH, Lee JM, Baek JH, Shin CI, Kiefer B, Han JK, Choi BI. Evaluation of hepatic fibrosis using intravoxel incoherent motion in diffusion-weighted liver MRI. J Comput Assist Tomogr. 2014; 38:110–6. [PubMed: 24378888]

37. Constandinou C, Henderson N, Iredale JP. Modeling liver fibrosis in rodents. Methods Mol Med. 2005; 117:237–250. [PubMed: 16118456]
38. Marques TG, Chaib E, da Fonseca JH, Lourenço AC, Silva FD, Ribeiro MA Jr, Galvão FH, D'Albuquerque LA. Review of experimental models for inducing hepatic cirrhosis by bile duct ligation and carbon tetrachloride injection. Acta Cir Bras. 2012; 27:589–94. [PubMed: 22850713]
39. Muriel P. Nitric oxide protection of rat liver from lipid peroxidation, collagen accumulation, and liver damage induced by carbon tetrachloride-Physiology, pathophysiology and pharmacology. Biochem Pharmacol. 1998; 56:773–779. [PubMed: 9751083]
40. Pagadala M, Kasumov T, McCullough AJ, Zein NN, Kirwan JP. Role of ceramides in nonalcoholic fatty liver disease. Trends Endocrinol Metab. 2012; 23:365–71. [PubMed: 22609053]
41. Lu J, Zhou J, Cai C, Cai S, Chen Z. Observation of true and pseudo NOE signals using CEST-MRI and CEST-MRS sequences with and without lipid suppression. Magn Reson Med. 2014; doi: 10.1002/mrm.25277
42. Jones CK, Huang A, Xu J, Edden RA, Schar M, Hua J, Oskolkov N, Zaca D, Zhou J, McMahon MT, Pillai JJ, van Zijl PC. Nuclear Overhauser enhancement (NOE) imaging in the human brain at 7T. Neuroimage. 2013; 77:114–24. [PubMed: 23567889]
43. Jin T, Wang P, Zong X, Kim SG. MR imaging of the amide-proton transfer effect and the pH-insensitive nuclear over hauser effect at 9.4 T. Magn Reson Med. 2013; 69:760–70. [PubMed: 22577042]
44. Li L, Tang X, Taylor KG, DuPré DB, Yappert MC. Conformational characterization of ceramides by nuclear magnetic resonance spectroscopy. Biophys J. 2002; 82:2067–80. [PubMed: 11916863]
45. Ichi I, Nakahara K, Fujii K, Iida C, Miyashita Y, Kojo S. Increase of ceramide in the liver and plasma after carbon tetrachloride intoxication in the rat. J Nutr Sci Vitaminol (Tokyo). 2007; 53:53–6. [PubMed: 17484380]
46. Ling W, Regatte RR, Navon G, Jerschow A. Assessment of glycosaminoglycan concentration in vivo by chemical exchange-dependent saturation transfer (gagCEST). Proc Natl Acad Sci (USA). 2008; 105:2266–2270. [PubMed: 18268341]
47. Heo HY, Zhang Y, Lee DH, Hong X, Zhou J. Quantitative assessment of amide proton transfer (APT) and nuclear Overhauser enhancement (NOE) imaging with extrapolated semi-solid magnetization transfer reference (EMR) signals: Application to a rat glioma model at 4.7 T. Magn Reson Med. 2015; doi: 10.1002/mrm.25581
48. Chow AM, Gao DS, Fan SJ, Qiao Z, Lee FY, Yang J, Man K, Wu EX. Measurement of liver T1 and T2 relaxation times in an experimental mouse model of liver fibrosis. J Magn Reson Imaging. 2012; 36:152–158. [PubMed: 22334510]
49. Stancanello J, Terreno E, Castelli DD, Cabella C, Uggeri F, Aime S. Development and validation of a smoothing-splines-based correction method for improving the analysis of CEST-MR images. Contrast Media Mol Imaging, 2008. 2008; 3:136–49.
50. Kim M, Gillen J, Landman BA, Zhou J, van Zijl P. Water saturation shift referencing (WASSR) for chemical exchange saturation transfer (CEST) experiments. Magn Reson Med. 2009; 61:1441–1450. [PubMed: 19358232]
51. Sun PZ, Benner T, Kumar A, Sorensen AG. Investigation of optimizing and translating pH-sensitive pulsed-chemical exchange saturation transfer (CEST) imaging to a 3T clinical scanner. Magn Reson Med. 2008; 60:834–841. [PubMed: 18816867]
52. Zaiss M, Schmitt B, Bachert P. Quantitative separation of CEST effect from magnetization transfer and spillover effects by Lorentzian-line-fit analysis of z-spectra. J Magn Reson. 2011; 211:149–155. [PubMed: 21641247]
53. Chappell MA, Donahue MJ, Tee YK, Khrapitchev AA, Sibson NR, Jezzard P, Payne SJ. Quantitative Bayesian model-based analysis of amide proton transfer MRI. Magn Reson Med. 2013; 70:556–567. [PubMed: 23008121]
54. Zaiss M, Xu J, Goerke S, Khan IS, Singer RJ, Gore JC, Gochberg DF, Bachert P. Inverse Z-spectrum analysis for spillover-, MT-, and T1-corrected steady-state pulsed CEST-MRI - application to pH-weighted MRI of acute stroke. NMR Biomed. 2014; 27:240–252. [PubMed: 24395553]

55. Zhao F, Deng M, Yuan J, Teng GJ, Ahuja AT, Wang YX. Experimental evaluation of accelerated T1rho relaxation quantification in human liver using limited spin-lock times. Korean J Radiol. 2012; 13:736–42. [PubMed: 23118572]

56. Wang YX, Zhao F, Yuan J, Mok GS, Ahuja AT, Griffith JF. Accelerated T1rho relaxation quantification in intervertebral disc using limited spin-lock times. Quant Imaging Med Surg. 2013; 3:54–8. [PubMed: 23482987]

57. Yuan J, Zhao F, Griffith JF, Chan Q, Wang YX. Optimized efficient liver T(1ρ) mapping using limited spin lock times. Phys Med Biol. 2012; 57:1631–40. [PubMed: 22398137]

58. Zhu Y, Zhang Q, Liu Q, Wang YX, Liu X, Zheng H, Liang D, Yuan J. PANDA- T1ρ: Integrating principal component analysis and dictionary learning for fast T1ρ mapping. Magn Reson Med. 2014; doi: 10.1002/mrm.25130

59. Sun PZ, Wang E, Cheung JS, Zhang X, Benner T, Sorensen AG. Simulation and optimization of pulsed radio frequency (RF) irradiation scheme for chemical exchange saturation transfer (CEST) MRI - demonstration of pH-weighted pulsed-amide proton CEST MRI in an animal model of acute cerebral ischemia. Magn Reson Med. 2011; 66:1042–1048. [PubMed: 21437977]

60. Zu Z, Li K, Janve VA, Does MD, Gochberg DF. Optimizing Pulsed-Chemical Exchange Saturation Transfer (CEST) Imaging Sequences. Magn Reson Med. 2011; 66:1100–1108. [PubMed: 21432903]

Key points

1. CEST MRI of *in-vivo* liver was demonstrated at clinical 3T field strength.
2. After 24-hour fasting, rat liver APTw and GlycoCEST signals decreased significantly.
3. After CCl4 intoxication both rat liver APTw and GlycoCEST signals decreased significantly.
4. Good scan-rescan reproducibility of liver CEST MRI was shown in healthy volunteers.

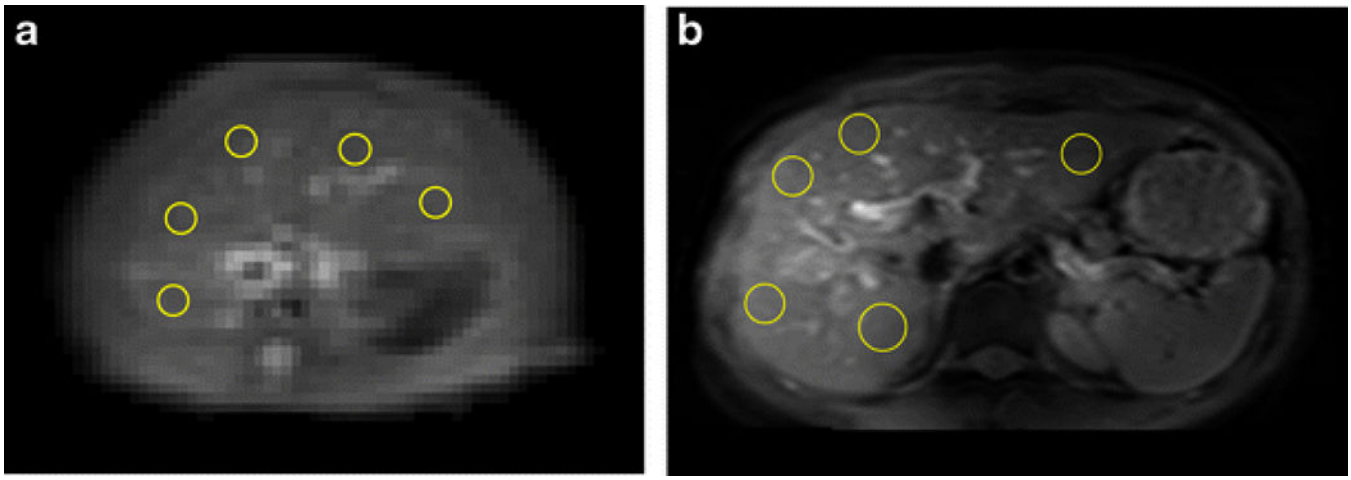

Fig. 1.

A&B. An example of placement of ROIs on a rat liver parenchyma region of T2 weighted image (A) and CEST image (B); C: An example of placement of ROIs on a human subject liver parenchyma region of CEST image. Artifacts and blood vessels were excluded.

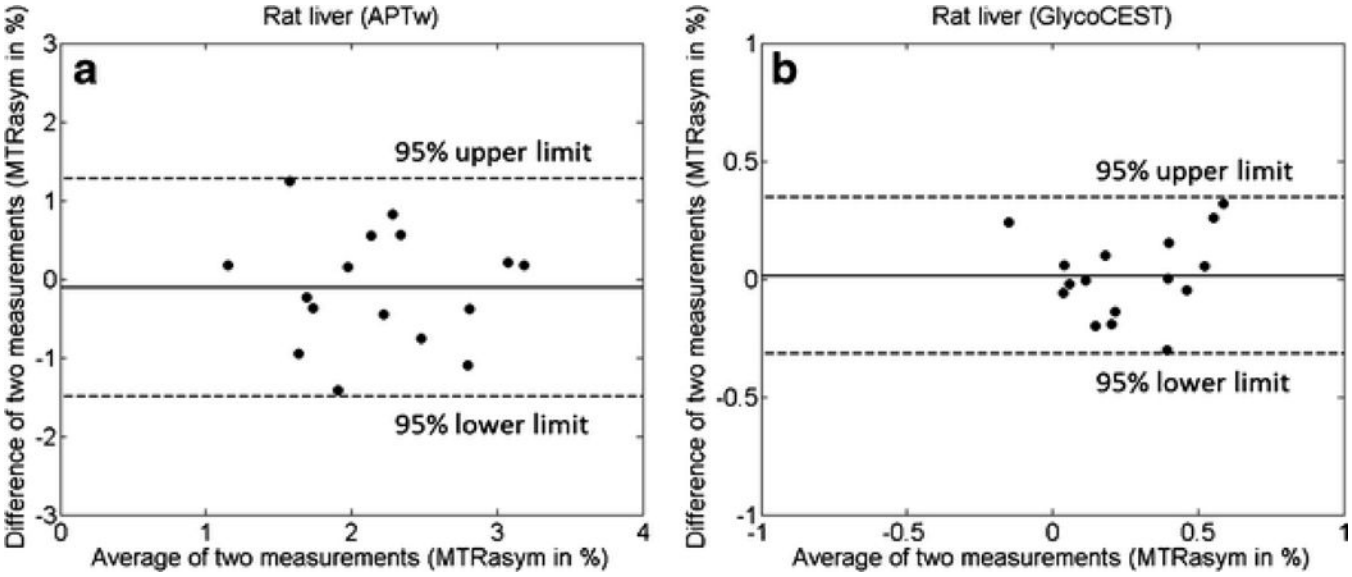

Fig. 2.

Bland-Altman plots for APTw (A) and GlycoCEST (B) imaging of 16 rats. The inter-scan differences of MTR_{asym} values are plotted against the average MTR_{asym} values of two scans for each rat.

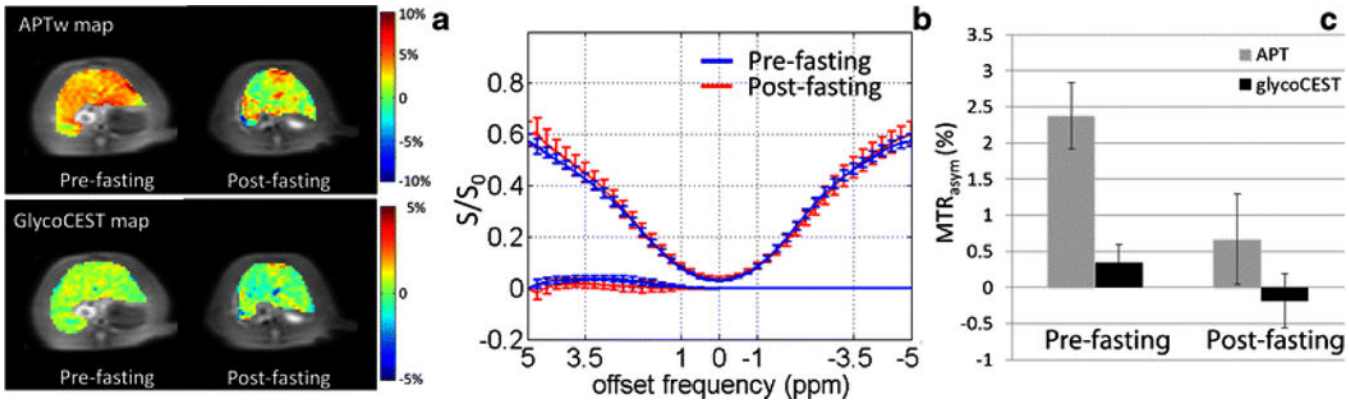

Fig. 3.

Typical APTw image and GlycoCEST image (A) of a rat liver before and after 24-hour fasting with the corresponding ROI-averaged Z-spectrum and MTR_{asym} spectrum (B). In this rat, the APTw MTR_{asym} was 3.67% and the GlycoCEST MTR_{asym} was 0.3% before 24-hour fasting. After 24-hour fasting, the APTw MTR_{asym} was 1.41% and the GlycoCEST MTR_{asym} was 0.04%. C: Bar plot of rat liver MTR_{asym} value of APTw and GlycoCEST before and after 24-hour fasting (n=8).

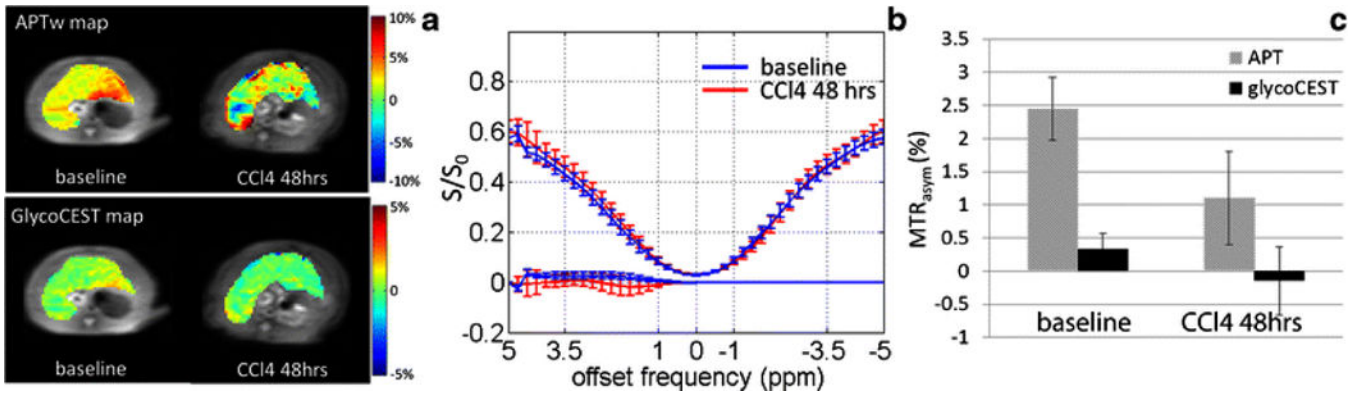

Fig. 4.

Typical APTw image and GlycoCEST image (A) of a rat liver before and after CCl4 injection with the corresponding ROI-averaged Z-spectrum and MTR_{asym} spectrum (B). In this rat, the baseline APTw MTR_{asym} was 2.66% and the GlycoCEST MTR_{asym} was 0.56%. After 48-hour CCl4 intoxication, the APTw MTR_{asym} was 1.91% and the GlycoCEST MTR_{asym} was -0.05%. C: Bar plot of rat liver MTR_{asym} value of APTw and GlycoCEST before and after 48-hour CCl4 injection (n = 11).

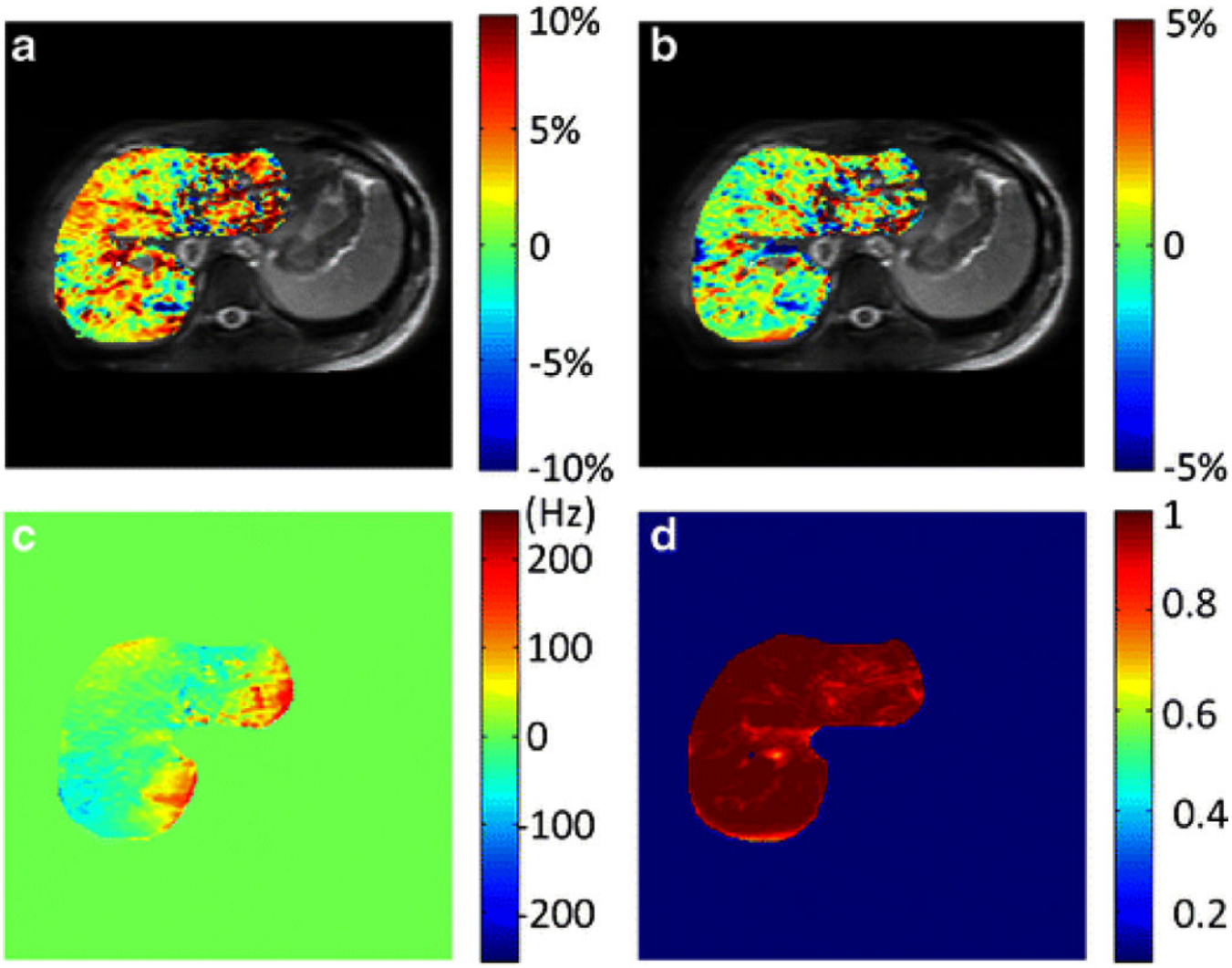

Fig. 5.

Liver APTw image (A), GlycoCEST image (B), ΔB_0 map (C) and R^2 map (D) in a healthy 24-year-old female volunteer.

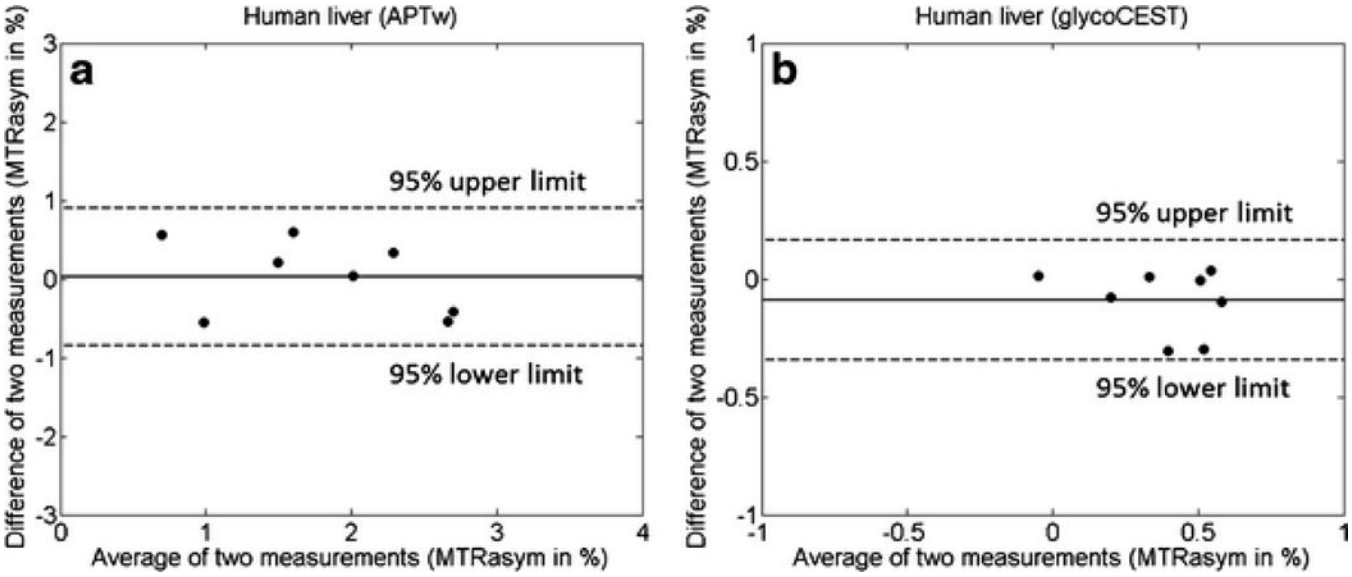

Fig. 6.

Bland-Altman plots for the liver APTw (A) and the liver GlycoCEST (B) of 8 healthy volunteers. The inter-scan differences of MTR_{asym} values are plotted against the average MTR_{asym} values of two scans for each subject.